Intranasal vaccination with influenza HA/GO-PEI nanoparticles provides immune protection against homo- and heterologous strains

Chunhong Dong[a], Ye Wang[a], Gilbert X. Gonzalez[a], Yao Ma[a], Yufeng Song[a], Shelly Wang[b], Sang-Moo Kang[a], Richard W. Compans[b], and Bao-Zhong Wang[a,1]

[a]Center for Inflammation, Immunity and Infection, Institute for Biomedical Sciences, Georgia State University, Atlanta, GA 30302; and [b]Department of Microbiology and Immunology, Emory University School of Medicine, Emory University, Atlanta, GA 30322

Edited by Peter Palese, Icahn School of Medicine at Mount Sinai, New York, NY, and approved April 5, 2021 (received for review December 6, 2020)

Intranasal (i.n.) immunization is a promising vaccination route for infectious respiratory diseases such as influenza. Recombinant protein vaccines can overcome the safety concerns and long production phase of virus-based influenza vaccines. However, soluble protein vaccines are poorly immunogenic if administered by an i.n. route. Here, we report that polyethyleneimine-functionalized graphene oxide nanoparticles (GP nanoparticles) showed high antigen-loading capacities and superior immunoenhancing properties. Via a facile electrostatic adsorption approach, influenza hemagglutinin (HA) was incorporated into GP nanoparticles and maintained structural integrity and antigenicity. The resulting GP nanoparticles enhanced antigen internalization and promoted inflammatory cytokine production and JAWS II dendritic cell maturation. Compared with soluble HA, GP nanoparticle formulations induced significantly enhanced and cross-reactive immune responses at both systemic sites and mucosal surfaces in mice after i.n. immunization. In the absence of any additional adjuvant, the GP nanoparticle significantly boosted antigen-specific humoral and cellular immune responses, comparable to the acknowledged potent mucosal immunomodulator CpG. The robust immune responses conferred immune protection against challenges by homologous and heterologous viruses. Additionally, the solid self-adjuvant effect of GP nanoparticles may mask the role of CpG when coincorporated. In the absence of currently approved mucosal adjuvants, GP nanoparticles can be developed into potent i.n. influenza vaccines, providing broad protection. With versatility and flexibility, the GP nanoplatform can be easily adapted for constructing mucosal vaccines for different respiratory pathogens.

recombinant protein vaccines | intranasal vaccination | graphene oxide nanoparticles | immunoenhancing effect | homologous and heterologous protection

Influenza remains one of the leading infectious diseases causing morbidity and mortality worldwide. Vaccination is the most cost-effective approach to preventing influenza virus infection. However, current virus-based seasonal influenza vaccines induce strain-specific immunity and are less effective against mismatched strains that may cause influenza epidemics (1). Furthermore, there is no vaccine countermeasure available for new pandemic strains. Intranasal (i.n.) immunization is a promising vaccination route for infectious respiratory diseases, such as influenza. This vaccination route can induce both systemic and mucosal immune responses. Secretory immunoglobulin A (sIgA) and immunoglobulin G (IgG) may prevent influenza infection at the portal of virus entry. Influenza mucosal immunity has been reported to confer cross-protection against heterologous and heterosubtypic viruses (2). Moreover, needle-free i.n. influenza vaccines possess superior logistical advantages over traditional injectable vaccines, such as easy administration with high acceptance for recipients and avoidance of biohazardous sharps waste.

However, the development of i.n. influenza vaccines has progressed slowly. The cold-adapted live-attenuated influenza virus (LAIV) vaccine is the only available human i.n. influenza vaccine up to date. Studies have shown that the LAIV vaccine could provide heterologous immunity (3). Nevertheless, safety concerns of LAIV are raised, especially in high-risk populations, such as infants under 2 y old and the elderly over 50. LAIV could undergo genetic reassortments and revert into a virulent form, thus posing a risk. Besides, the suboptimal protective efficacy of LAIV vaccines was reported in children in the 2009 H1N1 pandemic. A new generation of virus-independent, safe, and efficient influenza i.n. vaccines that induce broader cross-protection with high efficacy is urgently needed.

Intranasal vaccination with recombinant protein/peptide-based vaccines is an attractive strategy with high safety (4). Purified protein/peptide antigens eliminate safety concerns in individuals with egg allergies, possess minimal side effects, and enable quick and cost-effective production. However, soluble protein vaccines are poorly immunogenic by i.n. immunization due to the harsh and tolerogenic mucosal environment (5). The selection of appropriate formulations and adjuvants is crucial for successful i.n. vaccines. Nanoparticle vaccine platforms have been applied for i.n. vaccine development in recent years (6, 7). Nanoparticles serve as antigen and adjuvant carriers and immunostimulants themselves to enhance immune responses. The immunoenhancing effects of various nanoparticles have been reported (8–13). However, most

Significance

A noninvasive intranasal (i.n.) influenza vaccine can induce mucosal immune responses in respiratory tracts, preventing infection at the portal of virus entry. However, the absence of appropriate mucosal adjuvants at present hinders the development of such a vaccine. Here, we developed polyethyleneimine-functionalized two-dimensional graphene oxide nanoparticles (GP) that showed high antigen-loading capacities and superior immunoenhancing properties. Robust and broadly reactive immune responses were induced with i.n. immunization with GP-HA nanoparticles, conferring protection against homologous and heterologous viruses. With versatility and flexibility, GP nanoparticles can be easily adapted for constructing mucosal vaccines of different respiratory pathogens.

Author contributions: C.D. and B.-Z.W. designed research; C.D., Y.W., G.X.G., Y.M., Y.S., and S.W. performed research; C.D., Y.W., Y.M., Y.S., S.W., S.-M.K., and B.-Z.W. contributed new reagents/analytic tools; C.D., Y.W., G.X.G., S.-M.K., R.W.C., and B.-Z.W. analyzed data; C.D. and B.-Z.W. wrote the paper; and C.D., Y.W., G.X.G., Y.M., Y.S., S.W., S.-M.K., R.W.C., and B.-Z.W. revised the paper.

The authors declare no competing interest.

This article is a PNAS Direct Submission.

[1]To whom correspondence may be addressed. Email: bwang23@gsu.edu.

This article contains supporting information online at https://www.pnas.org/lookup/suppl/doi:10.1073/pnas.2024998118/-/DCSupplemental.

Published May 3, 2021.

nanoparticle vaccines suffer from low antigen-loading capacity, complicated and lengthy preparation procedures, and structural complexity because of covalent conjugation.

Two-dimensional (2D) graphene oxide (GO) nanoparticles have great potential as a novel vaccine platform due to their extraordinary attributes. These features include the high aspect ratio and ultra-large surface area for high-density antigen association, wealthy chemical groups for flexible surface modification and noncovalent antigen loading via electrostatic adsorption, hydrogen bond, and hydrophobic and π–π stacking interactions. Besides, GO nanoparticles themselves are biocompatible and nonimmunogenic (14, 15). Various GO vaccine formulations were demonstrated to induce improved immune responses by activating immune cells or triggering innate signaling (16–18). However, most prior studies were limited to conventional routes with tumor antigens for cancer immunotherapies. Studies on GO-based influenza i.n. vaccines are lacking.

We developed a polyethyleneimine (PEI)-functionalized GO (GO-PEI, GP) influenza vaccine nanoplatform, prepared influenza GP nanoparticles by incorporating recombinant influenza hemagglutinin (HA) and investigated their immunoenhancing effects (Fig. 1). Our work revealed that influenza GP nanoparticles enhanced antigen internalization and promoted the production of inflammatory cytokines and the maturation of JAWS II dendritic cells (DCs) during in vitro experiments. i.n. vaccination with influenza GP nanoparticles induced robust humoral and cellular immune responses, conferring broader protection against challenges by homologous and heterologous influenza viruses in mice.

Results

Fabrication and Characterization of GO Nanoparticle Vaccines. GO nanoparticle vaccines can be prepared in several approaches (19, 20). We found that simple mixtures of naked GO and proteins are prone to precipitation, and the protein loading capacity is low by direct surface adsorption. One of the best ways to engineer GO-based vaccine delivery systems is surface functionalization, which tailors the interactions between GO nanoparticles, vaccine components, and biosurfaces and adjusts the adjuvant activity. In this study, we functionalized GO with a cationic polymer, branched PEI, to construct GP nanoparticles and investigated their immunoenhancing effects (Fig. 1). Positively charged nanoparticles are especially suitable for mucosal vaccination (21). Recent studies showed that PEI has a potent mucosal adjuvant effect (22).

The pristine GO nanoparticles were prepared by tip sonication of GO flakes in an ice bath. The GO flakes gradually became smaller nano-sized GO nanoparticles upon sonication (*SI Appendix*, Fig. S1*A*), and the final nanoparticles were around 164 nm. Transmission electron microscopy (TEM) and atomic force microscopy (AFM) images revealed the sheet-like morphology and uniform size distribution of the GO nanoparticles (Fig. 2*A* and *SI Appendix*, Fig. S1*B*). We prepared GP nanoparticles using the Carbodiimide coupling method. The thermogravimetric analysis (TGA) indicated that 17.94% PEI was conjugated on the GP nanoparticles (*SI Appendix*, Fig. S1*C*). The resulting GP nanoparticles were 185 ± 1.94 nm (Fig. 2*C*). From pristine GO to positive GP, the surface charge changed from negative (−38.5 ± 0.51 mV) to positive (66.97 ± 1.65 mV) (Fig. 2*D*), facilitating a high loading capacity of the protein antigens by direct electrostatic adsorption without chemical conjugation. Notably, compared with GO nanoparticles, GP has improved dispersibility and stability in saline solutions. PEI-functionalized GO was reported to be biocompatible (23).

We have previously demonstrated that GCN4-stabilized trimetric influenza HA possesses enhanced immunogenicity compared with

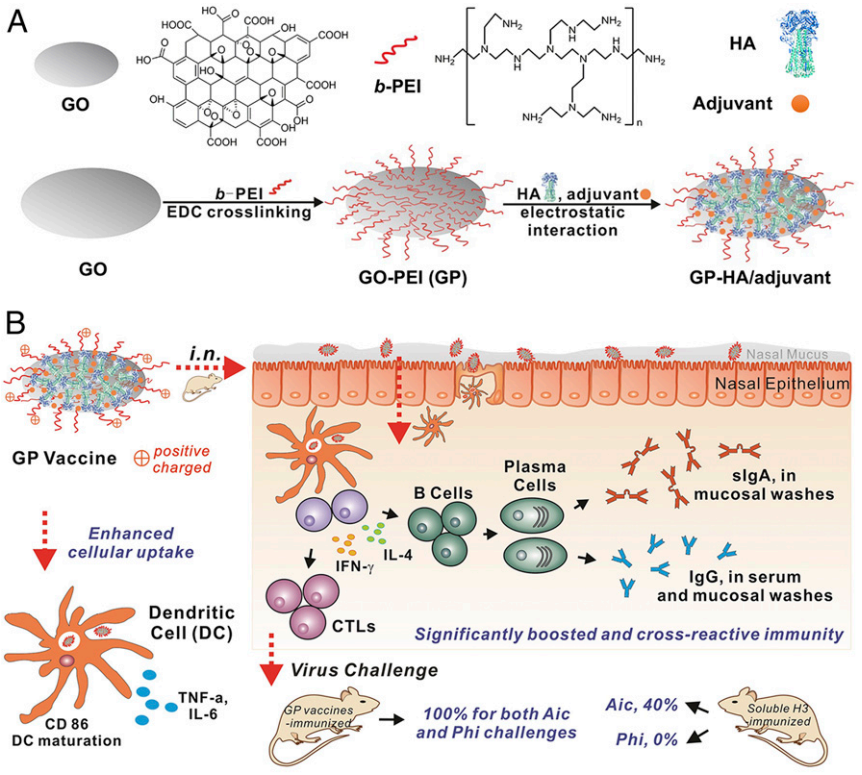

Fig. 1. Schematic illustration of the preparation and performance of influenza GP nanoparticles. (*A*) Preparation of GP and GP-HA/adjuvant nanoparticles. (*B*) Immunoenhancing effects of GP nanoparticle vaccines. GP nanoparticle vaccines showed enhanced cellular uptake in DCs and promoted inflammatory cytokine secretion and DC maturation. i.n. vaccination with influenza GP nanoparticles induced significantly enhanced and broad immune protection against homo- and heterologous influenza virus challenges. CTL, cytotoxic T lymphocyte; SR, survival rate.

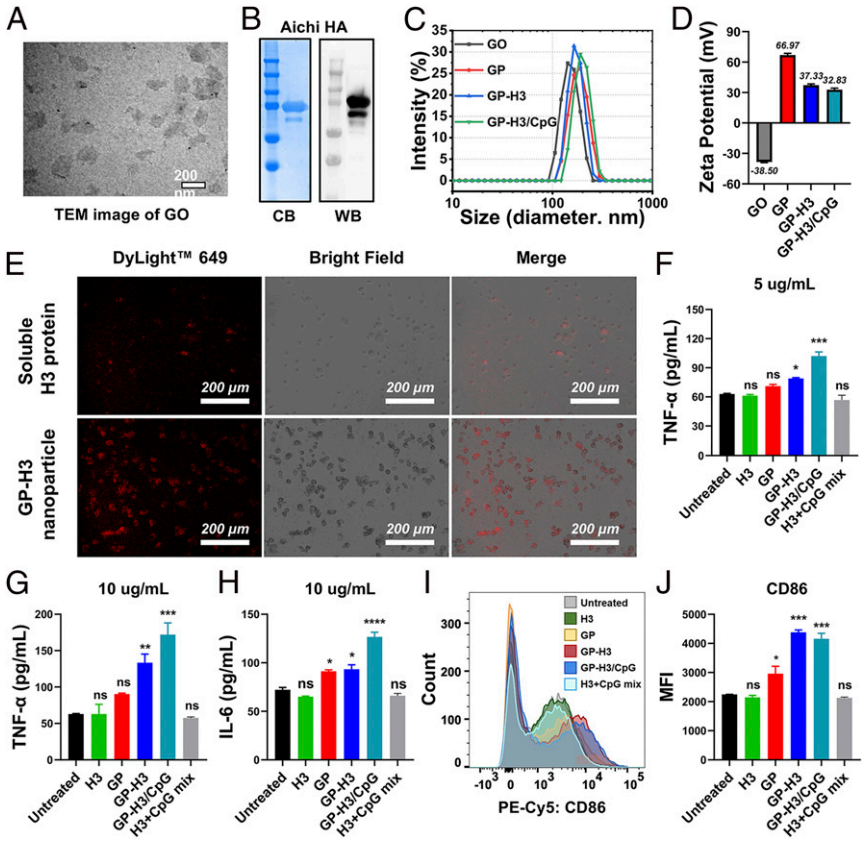

Fig. 2. Characterization of the influenza GP nanoparticles. (*A*) TEM image of GO nanoparticles. (*B*) Coomassie blue staining (CB) and Western blotting (WB) analysis. (*C* and *D*) Nanoparticle size and Zeta-potential analysis. (*E*) Antigen internalization into JAWS II DCs by immunofluorescence. Intracellular H3 was probed by fluorescent-labeled antibodies (red). (*F–H*) Proinflammatory cytokine production of JAWS II cells treated with different formulations at indicated H3 concentrations. (*I* and *J*) CD86 expression on JAWS II cells by flow cytometry. MFI, mean fluorescence intensity. The data are presented as mean ± SEM. The statistical significance was analyzed by one-way ANOVA followed by Dunnett's multiple comparison test, comparing the mean of each group with the mean of the control group (Untreated) (*$P < 0.05$; **$P < 0.01$; ***$P < 0.001$; ****$P < 0.0001$; ns represents no significance, $P > 0.05$).

monomeric HA (24). We purified recombinant trimeric Aichi HA (A/Aichi/2/1968 (Aic), H3N2, designated H3) with high purity, as determined by sodium dodecyl sulfate–polyacrylamide gel electrophoresis (SDS-PAGE) followed by Coomassie Blue staining (Fig. 2*B*). The retention of HA antigenicity was verified by Western blotting analysis with antibodies. The trimeric state of H3 was determined by bis[sulfosuccinimidyl] suberate (BS3) cross-linking, followed by Western blots (*SI Appendix*, Fig. S2*A*). A main band with a threefold molecular weight of the monomeric HA was seen after a high concentration of BS3 (>5 mM) treatment to fix the polymeric HA, indicating the dominant trimeric state of the purified H3.

We generated GP nanoparticle vaccine formulations by a simple mixing/adsorption approach, as diagrammed in Fig. 1*A*. H3 was bound onto the large surface of GP nanoparticles mainly via electrostatic interactions. The antigen-loading capability of GP nanoparticles was evaluated by SDS-PAGE. At higher ratios of GP to H3 (2:1, 1:1, and 1:2), there were strong H3 bands from the nanoparticles without visible signals from the supernatants (*SI Appendix*, Fig. S2*B*), indicating the tight binding of H3 onto the GP nanoparticles. Some free H3 was present in the supernatants from lower GP:H3 ratios, indicating an excessive amount of H3 in this circumstance. The resulting GP-H3 nanoparticles had strong colloidal stability, especially at higher GP:H3 ratios. Ultraviolet-visible (UV-Vis) absorption spectra analysis in *SI Appendix*, Fig. S2*C* further confirmed the tight binding of H3 on GP nanoparticles. The results demonstrated that GP nanoparticles with positive charges and ultra-large surface areas could serve as protein antigen carriers with high antigen-loading capacities.

CpG ODN is a potent mucosal immunomodulator for the induction of antigen-specific cell-mediated immunity and humoral immune responses. We used CpG ODN1826 as a positive control group in our work. Meanwhile, negatively charged CpG molecules could be easily coloaded with influenza HA onto the GP particles to generate adjuvanted nanoparticles. Agarose gel electrophoresis was employed to investigate whether all the feeding CpG were complexed and loaded onto the GP nanoparticles. As shown in *SI Appendix*, Fig. S2*D*, strong CpG signals were observed from free CpG and H3+CpG but not from the supernatants of GP-H3/CpG (10:5:1) and GP-H3/CpG (10:5:2.5). The results indicated that all the feeding CpG was coloaded with H3 on the GP nanoparticles via electrostatic adsorption interaction. Additionally, the obtained GP-H3/CpG (10:5:1) nanoparticles displayed a Zeta-potential value of 32.83 ± 0.49 mV (Fig. 2*D*), which indicated that the resulting nanoparticles retained positive charges after loading with H3 and CpG. For subsequent studies, a GP:H3:CpG ratio of 10:5:1 was used for fabricating GP vaccine nanoparticles. The resulting GP-H3 and GP-H3/CpG nanoparticles ranged from 170 to 200 nm in diameter (Fig. 2*C*) and exhibited Zeta potentials of >+30 mV (Fig. 2*D*). The results demonstrated that GP-based H3 vaccine nanoparticles could be generated by the facile mixing method with appreciable particle features for i.n. immunization.

Effects on Murine DC Line JAWS II. Effective antigen uptake by DCs is critical for inducing potent immune responses. We detected

H3 internalization by immunofluorescence imaging in JAWS II cells treated with soluble H3 versus GP-H3 nanoparticles. The weak background fluorescence in the untreated cell controls indicated low nonspecific adsorption of fluorescent antibodies (*SI Appendix*, Fig. S3*A*). Soluble H3-treated JAWS II cells showed a weak fluorescence, indicating the low internalization of the H3 protein (Fig. 2*E*). In comparison, GP-H3 nanoparticle-treated cells displayed strong fluorescence, demonstrating significantly enhanced antigen-uptake efficacy in DCs. Besides, the immunofluorescence imaging results also confirmed that the specificity and function of H3 on GP-H3 nanoparticles were well maintained after loading on GP. These results revealed that GP-based HA nanoparticles were readily taken in by DCs.

Mature DCs produce cytokines to facilitate the activation and differentiation of T cells and regulate adaptive immunity. We evaluated the secreted cytokine (IL-6 and TNF-α) levels from JAWS II cells treated with different vaccine formulations. As shown in Fig. 2 *F* and *G*, soluble H3, GP, or H3+CpG induced comparable TNF-α secretion levels to the control, while GP-H3 and GP-H3/CpG nanoparticles induced significantly higher levels of TNF-α secretion at both H3 concentrations. Meanwhile, soluble H3 and H3+CpG groups showed similar IL-6 production levels to the control group in JAWS II cells (Fig. 2*H*). In comparison, GP or GP-H3 treatment significantly enhanced IL-6 production ($P < 0.05$). The low TNF-α and IL-6 secretion in the H3+CpG group could indicate the limited internalization of the soluble protein and CpG into JAWS II cells. Although soluble CpG did not influence cytokine production, CpG-loaded GP-H3/CpG nanoparticles showed a substantial enhancement over GP-H3 nanoparticles. Among all groups, GP-H3/CpG treatment induced the highest cytokine production in JAWS II cells. Therefore, GP vaccine nanoparticles enormously boosted the production of proinflammatory cytokines in JAWS II cells.

We studied the maturation efficacy of JAWS II cells by evaluating a DC maturation marker CD86 with flow cytometry. Consistent with the cytokine secretion results, soluble H3 or H3+CpG-treated JAWS II cells showed background levels of CD86 expression (Fig. 2 *I* and *J*). In contrast, GP-H3 and GP-H3/CpG treatments showed significantly higher CD86 expression ($P < 0.001$), as revealed by the redshift of the fluorescence spectra and the enhanced mean fluorescence intensity. Interestingly, naked GP nanoparticle treatment enhanced the CD86 expression ($P < 0.05$), demonstrating GP nanoparticles' adjuvant effect. Overall, these results showed that GP nanoparticles could be readily internalized by DCs and promote the production of proinflammatory cytokines, IL-6 and TNF-α, and stimulate DC maturation.

Induction of Humoral Immune Responses. We investigated the GP-H3 nanoparticle immunogenicity by a two-dose vaccination scheme (Fig. 3*A*). Immunization groups include soluble H3, GP-H3, GP-H3/CpG, and H3+CpG (5 μg of H3 per mouse). A previous study showed that a single i.n. dose of 10 or 20 μg of PEI was similarly safe as cholera holotoxin, CTB, and poly(lactic-coglycolic acid) nanoparticles used at or above standard doses (22). In the present study, the PEI amount on GP nanoparticles was 1.79 μg per mouse (10 μg GP per mouse) determined by the TGA results.

Serum antigen-specific IgG levels were titrated (Fig. 3 *B* and *C*). The results demonstrated that the soluble H3 group displayed a low seroconversion efficiency and a low serum IgG level after the immunization. In contrast, GP-H3 nanoparticle immunization induced rapid seroconversion and significantly higher antigen-specific IgG antibody titers in both prime sera ($P < 0.01$) and boost sera ($P < 0.001$). H3+CpG significantly promoted the serum IgG responses compared to soluble H3, consistent with the previous studies (25). CpG has been proved in trials to accelerate the induction and generation of higher protective antibody titers with protein vaccines (26–28). All the GP nanoparticle (GP-H3 and GP-H3/CpG)–vaccinated mice showed high serum antigen-specific IgG titers after the boosting immunization. However, no significant difference was observed between GP-H3, GP-H3/CpG, and H3+CpG in antibody production.

Hemagglutination-inhibition (HAI) titer correlates to HA-induced immune protection. A serum HAI titer ≥40 is considered protective (29). As shown in Fig. 3*D*, soluble H3-immunized mice displayed relatively low HAI titers. In contrast, GP-H3 nanoparticles induced significantly higher HAI titer ($P < 0.0001$) than the H3 group. Although GP-H3/CpG group showed elevated HAI titers compared to GP-H3 and H3+CpG groups, the difference is not significant.

Antibodies can be neutralizing or nonneutralizing. Neutralizing antibodies inhibit viral infectivity by tightly binding to important viral structures and correlate immune protection for many vaccines (30). As shown in Fig. 3*E*, significantly higher Aic virus-specific neutralization antibody titers were induced in GP-H3 ($P < 0.0001$), GP-H3/CpG ($P < 0.0001$), and H3+CpG mix ($P < 0.0001$) groups compared to the soluble H3 group. H3 in GP nanoparticles induced comparable neutralizing activity to H3+CpG mix ($P > 0.05$), and CpG added no advantage when coincorporated into GP nanoparticles with H3 ($P > 0.05$). The antibody neutralization result was consistent with the antibody and HAI titer results.

I.n. vaccination can induce mucosal immunoglobulin A (IgA) and IgG in the respiratory tract surfaces, preventing influenza infection at the viral entry site. The cross-reactive sIgA provided broad protection against heterologous and heterosubtypic influenza viruses (31). As shown in Fig. 3 *F* and *G*, soluble H3 induced low levels of sIgA in nasal washes and bronchoalveolar lavage fluid (BALF). By contrast, GP-H3 and GP-H3/CpG nanoparticle groups displayed elevated IgA antibody levels, which are also higher than that of the H3+CpG mix group. We also observed high IgG levels in BALF (Fig. 3*H*) but not in nasal washes. These results were consistent with the previous observations that sIgA dominated the upper respiratory tract antibody response, whereas IgG was the major antibody isotype in the lower respiratory tracts (32). We observed that GP-H3 and GP-H3/CpG nanoparticles induced significantly higher IgG levels ($P < 0.01$, Fig. 3*H*) and HAI titers ($P < 0.001$, *SI Appendix*, Fig. S3*B*) in BALF than soluble H3, comparable to the H3+CpG mix group, but HAI titers were not detected in nasal washes from all groups (*SI Appendix*, Fig. S3*B*).

These results demonstrated that GP nanoparticles potently boosted antibody immune responses not only in systemic compartments but also at local mucosal surfaces. Coloading CpG to GP nanoparticles with H3 did not further significantly strengthen antigen-specific antibody responses, indicating that GP nanoparticle is a robust adjuvant system itself and may mask the adjuvant effect of CpG. We observed similar results from self-assembled protein nanoclusters in previous studies (33).

Induction of Cellular Immune Responses. Cellular immunity plays a crucial role in the battle against influenza infection. Early cytokine production in vaccination programs the dimension and magnitude of antigen-specific immune responses. We evaluated IL-4–secreting cell frequencies in spleen and cervical lymph node (CLN) lymphocytes 3 wk after boosting immunization. As shown in Fig. 4*A*, we observed significantly increased numbers of IL-4–secreting splenocytes in the GP-H3 ($P < 0.001$) and GP-H3/CpG ($P < 0.0001$) nanoparticle groups versus the soluble H3 or H3+CpG mix groups. We found no significant difference between soluble H3 and H3+CpG groups in the number of IL-4–secreting splenocytes ($P > 0.05$). Similarly, GP nanoparticles boosted the IL-4–secreting lymphocyte generation in CLNs of vaccinated mice (Fig. 4*B*). Meanwhile, IFN-γ–producing lymphocytes were also observed in spleens and CLNs of nanoparticle-immunized

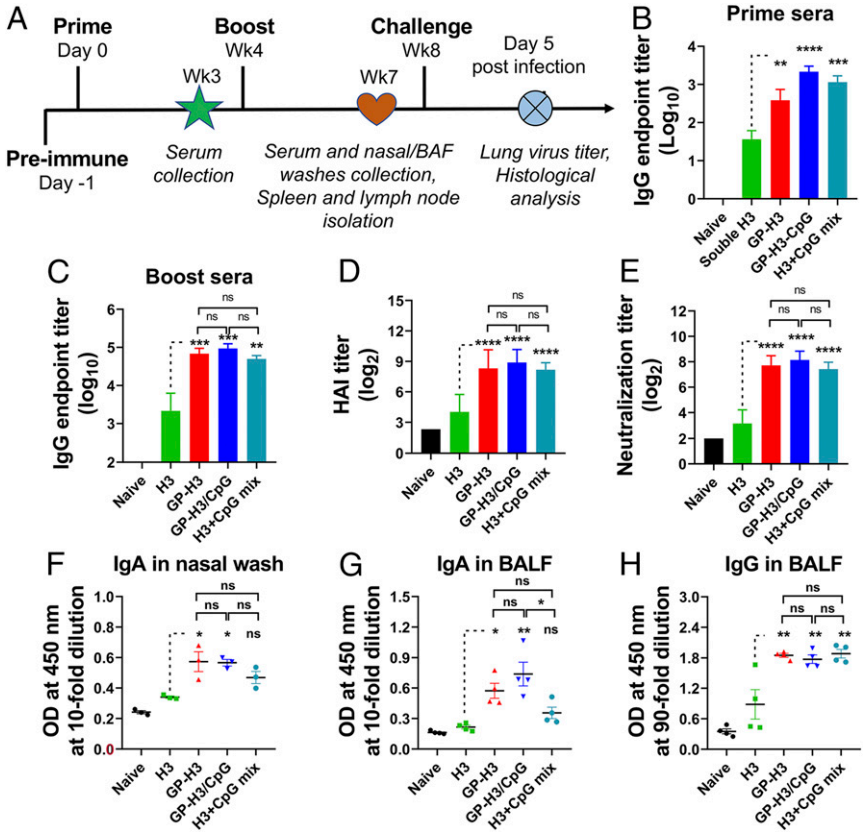

Fig. 3. Humoral immune responses. (*A*) Timeline of immunization, sample collection, and challenge experiments. BALB/c mice were i.n. immunized twice in a 4-wk interval. Groups included soluble H3, GP-H3, GP-H3/CpG, and H3+CpG mix. Naïve mice were used as controls. (*B* and *C*) Aic-specific IgG endpoint titers in mice prime and boost sera, respectively. (*D* and *E*) HAI and neutralization titers in mouse boost sera. (*F* and *G*) Optical density (OD) values at 450 nm for diluted nasal washes and BALF samples to detect mucosal IgA by ELISA. (*H*) OD values at 450 nm for diluted BALF samples to detect mucosal IgG. The data are presented as mean ± SEM. The statistical significance was analyzed by one-way ANOVA followed by Tukey's multiple comparison test, comparing the mean of each group with the mean of the H3 group (*$P < 0.05$; **$P < 0.01$; ***$P < 0.001$; ****$P < 0.0001$; ns represents no significance, $P > 0.05$).

mice. GP-H3 nanoparticle immunization induced significantly more IFN-γ–producing lymphocytes than soluble H3 (*SI Appendix*, Fig. S4 *A* and *B*). Considering the abundant IL-4–secreting cells observed, we measured the IgE antibody levels in boost sera. GP-H3 nanoparticle–vaccinated mice showed similar low IgE levels to the soluble H3 group (*SI Appendix*, Fig. S4*C*). Besides, no visible inflammation was observed in the mouse nasal cavity 24 h post-i.n. immunization with GP-H3 nanoparticles (*SI Appendix*, Fig. S5*A*). We also did not find apparent mouse body weight changes and inflammatory cell infiltration in lungs 7 d post-immunization (*SI Appendix*, Fig. S5 *B* and *C*).

IL-4 facilitates B cell proliferation and differentiation into antibody-secreting plasma cells (ASCs) (34). We studied the antigen-specific IgG and IgA ASCs in mouse spleens and analyzed whether IL-4–secreting lymphocyte frequency correlates with the antibody induction. As shown in Fig. 4 *C* and *D*, compared with soluble H3, GP-H3 and GP-H3/CpG nanoparticles induced increased numbers of H3-specific IgG and IgA ASCs in splenocytes. We also observed a similar plasma B cell pattern in nasal-associated lymphoid tissues (NALTs) (*SI Appendix*, Fig. S5*D*). Therefore, GP nanoparticles significantly boosted antigen-specific plasma B cell generation.

We evaluated CD4+ and CD8+ T cell proliferation in splenocytes by the carboxyfluorescein succinimidyl ester (CFSE) staining assay (Fig. 4 *E–H* and *SI Appendix*, Fig. S6). While all immunization groups showed a noticeable decrease in cellular CFSE fluorescence intensity over controls, higher CD4+ and CD8+ T cell proliferation was elicited in GP-H3 and GP-H3/CpG groups versus the soluble H3 group. We also analyzed CD4+ and CD8+ T cell percentages in splenocytes after antigen restimulation (*SI Appendix*, Fig. S7). Both GP-H3 and GP-H3/CpG groups displayed higher CD4+ and CD8+ T cell rates than the soluble H3 group in the bulk splenocytes. Therefore, GP nanoparticle vaccination significantly promoted cellular immune response, indicating the appreciable adjuvanticity of GP nanoparticles. Although CpG improved T cell responses in the context of H3+CpG mix, we did not observe the adjuvant effect in GP-H3/CpG nanoparticles (Fig. 4 *E–H*).

Protective Efficacy against Homologous Influenza Virus Challenge. We investigated the prophylaxis efficiency of different formulations by challenging mice with 15× median lethal dose (LD_{50}) Aic (Fig. 5 *A* and *B*) 4 wk post-boosting immunization. The soluble H3 immunization conferred partial protection (40% mouse survival) with apparent body weight loss (*SI Appendix*, Fig. S8*A*). By contrast, mice in GP-H3, GP-H3/CpG, and H3+CpG mix immunization groups survived the challenge without significant weight loss. These results demonstrated that GP nanoparticle vaccines displayed superior protective effects versus soluble H3.

We performed histological examinations and determined lung virus titers 5 d postchallenge. Naïve and soluble H3-immunized mice demonstrated a severe inflammatory state with massive tissue damage and leukocyte infiltration (Fig. 5*C*). By contrast, GP nanoparticle (GP-H3 and GP-H3/CpG) and H3+CpG mix immunized mice displayed a nearly normal state with significantly decreased leukocyte infiltration (Fig. 5 *C* and *D*). Additionally,

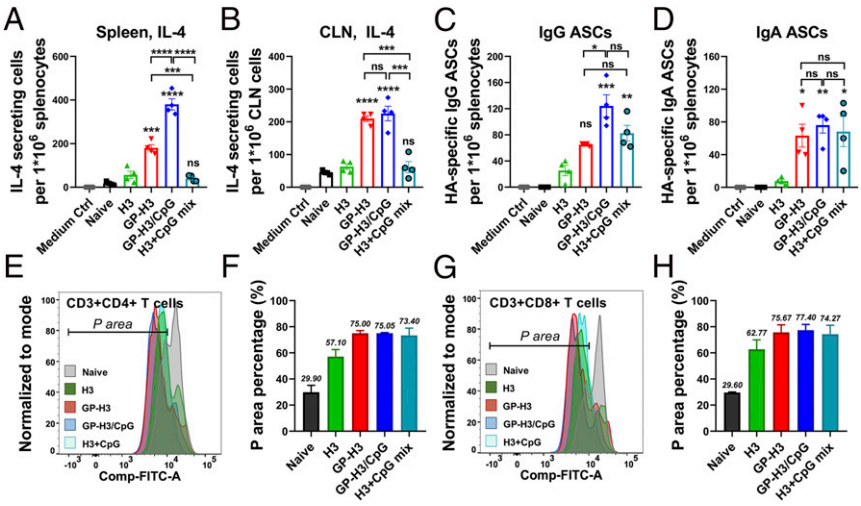

Fig. 4. Cellular immune responses. (*A* and *B*) IL-4–secreting cells in splenocytes and CLN cells. (*C* and *D*) Antigen-specific IgG and IgA plasma cells in splenocytes. (*E* and *F*) CD3+CD4+ T cell proliferation by CFSE staining assay. (*G* and *H*) CD3+CD8+ T cell proliferation. The population with decreased fluorescence intensity of CFSE was labeled as P area, representing the cells that have undergone proliferation. The data are presented as mean ± SEM. The statistical significance was analyzed by one-way ANOVA followed by Tukey's multiple comparison test, comparing the mean of each group with the mean of a control group (H3) (*$P < 0.05$; **$P < 0.01$; ***$P < 0.001$; ****$P < 0.0001$; ns represents no significance, $P > 0.05$).

H3-immunized mice also displayed high lung virus titers ($1 \times 10^{4.83}$ tissue culture infective doses [$TCID_{50}$]). In contrast, GP-H3, GP-H3/CpG, and H3+CpG mix groups showed undetectable lung virus titers (Fig. 5*E*). These results demonstrated that GP nanoparticle-induced immune responses significantly inhibited viral replication in mouse lungs, comparable to H3+CpG mix.

We measured the inflammatory cytokine (TNF-α, IL-12, and IL-6) levels in the BALF samples to evaluate the pulmonary immunopathology. As shown in Fig. 5 *F–H*, both naïve and soluble H3-immunized mice produced high levels of TNF-α, IL-12, and IL-6 after virus infection. In comparison, the mice in the GP-H3, GP-H3/CpG, and H3+CpG mix groups displayed significantly reduced TNF-α, IL-12, and IL-6 levels. We also detected substantially higher Aic virus-specific IgA and IgG antibody levels in BALF samples of infected mice in the GP nanoparticle-immunized groups (*SI Appendix*, Fig. S8*B*).

These results demonstrated the GP-H3 nanoparticles without an adjuvant provided complete protection in mice against Aic virus infection. GP nanoparticles showed great promise in boosting the immune responses of influenza HA and providing protection against influenza virus infection, comparable to the model adjuvant CpG. The GP nanoparticles may be a potent i.n. vaccine platform to bring recombinant protein vaccines into clinical applications when rare adjuvants are available for this purpose (CpG is still a laboratory adjuvant for vaccination studies at present).

Protective Efficacy against Heterologous Influenza Virus Challenge. We employed the heterologous A/Philippines/2/1982 (Phi, H3N2) virus to study the cross-protective effect conferred by GP nanoparticle i.n. vaccination. Immunized mice were challenged with 2× LD_{50} of Phi virus 4 wk post-boosting immunization. As shown in Fig. 6 *A* and *B* and *SI Appendix*, Fig. S9*A*, all mice in the soluble H3 group suffered rapid and severe weight loss and died in days 7 ~ 9 postchallenge, the same as the naïve control group. GP-H3, GP-H3/CpG, and H3+CpG mix groups showed full protection with slight weight loss.

A comparative analysis of Aic and Phi HA amino acid sequences showed a difference of 8.48%, representing a substantial antigenic drift (*SI Appendix*, Table S1). We investigated the cross-reaction and neutralization activities of mice immune serum against Phi. As shown in Fig. 6*C*, GP nanoparticles (GP-H3, GP-H3/CpG) and H3+CpG mix induced significantly higher Phi virus-specific IgG antibody titers in mouse sera than soluble H3. However, no apparent cross-neutralization titers were observed in all groups (*SI Appendix*, Fig. S9*B*). GP nanoparticles also induced higher Phi virus-specific IgA levels in nasal washes and higher IgG and IgA levels in BALF (Fig. 6 *D–F*). Interestingly, the GP-H3 nanoparticle-induced cross-reactive mucosal IgA titers were higher than that in H3+CpG mix group. No noticeable cross-reactive HAI titers against Phi virus were detected in sera or BALF of all groups (*SI Appendix*, Fig. S9*C*). We measured antibody titers specific to the head-removed Aic HA stalk protein (hrHA3) and observed significantly higher antibody titers in GP-H3 and GP-H3/CpG nanoparticle groups than the soluble H3 group (Fig. 6*G*). An enzyme-linked immunosorbent assay (ELISA) assay using an irrelevant his-tagged SARS-CoV-2 spike protein receptor-binding domain (RBD) as the coating antigen excluded the influence of the his-tag on hrHA3 (*SI Appendix*, Fig. S9*D*). HA-loaded GP nanoparticles significantly induced HA stalk-specific antibodies, contributing to the heterologous protection against the Phi virus.

We evaluated the cytokine-secreting splenocytes. Under the stimulation with inactivated Phi viruses, GP nanoparticle groups showed significantly higher IL-4– and IFN-γ–secreting splenocyte populations (Fig. 6 *H* and *I*). In contrast, the soluble H3 group demonstrated few such splenocytes.

Next, we studied cross-reactive antibody levels in immune sera and mucosal washes against A/Wisconsin/15/2009 (H3N2, Wis) and reassortant A/Shanghai/2/2013 (H7N9, rSH) from HA phylogenic Group 2. GP-H3 and GP-H3/CpG nanoparticles induced significantly higher serum IgG antibodies specific to Wis and rSH than soluble H3, while antibody levels specific to rSH were much lower than that to Wis (*SI Appendix*, Figs. S10*A* and S11*A*). We observed elevated mucosal antibody (IgG and IgA) levels specific to Wis from the GP nanoparticle groups (*SI Appendix*, Fig. S10 *B–D*) in contrast to the low or undetectable antibody levels to rSH (*SI Appendix*, Fig. S11 *B–D*). The results indicated that GP-H3 nanoparticles might confer better protection against heterologous strains in the same subtype but limited protection against heterosubtypic viruses (such as H7 subtype viruses) even from the same HA group.

Discussion

Broadly protective influenza vaccines are urgently needed due to the continuous antigenic drift and shift of influenza viruses.

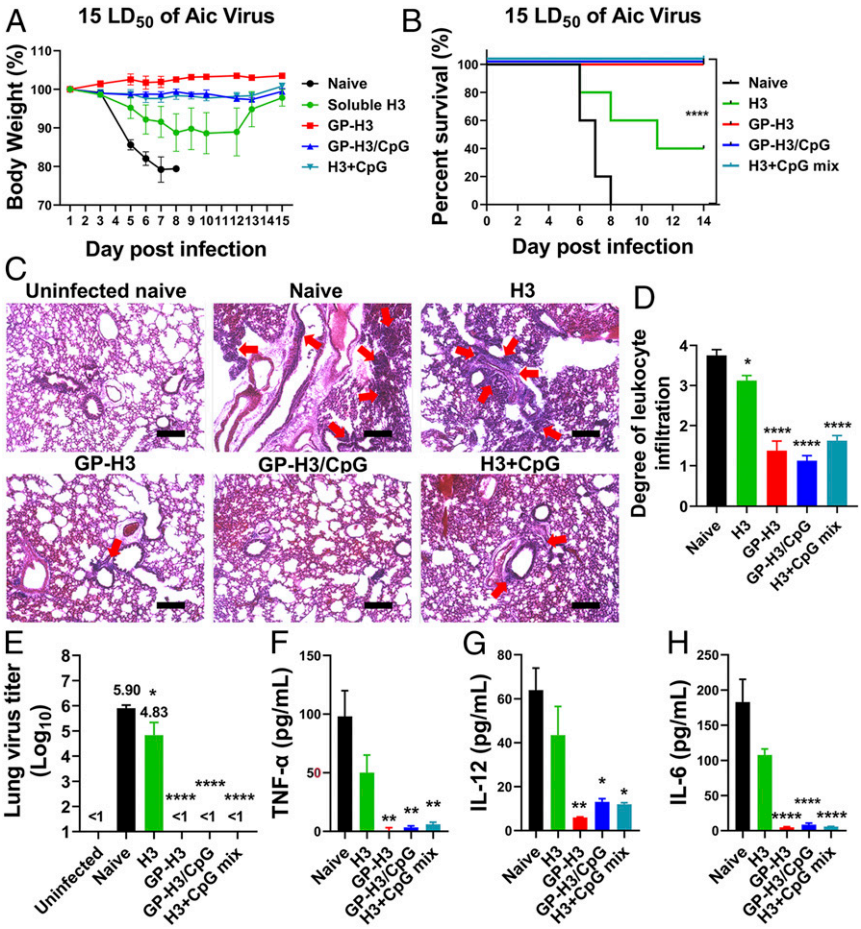

Fig. 5. Protective efficacy against homologous influenza virus challenge. (*A*) Morbidity and (*B*) mortality of mice after challenge. (*C*) Histological pathology analysis by H&E staining. The uninfected mouse lung section was used as a negative control. The red arrows in images indicate leukocyte infiltration. Images are representatives from each group. (Scale bars, 200 μm.) (*D*) Bar chart showing the scores of leukocyte infiltration degree. (*E*) Determination of mouse lung virus titers. (*F–H*) Evaluation of inflammatory cytokine (TNF-α, IL-12, and IL-6) levels in BALF of infected mice. The data are presented as mean ± SEM. The statistical significance was analyzed by one-way ANOVA followed by Dunnett's multiple comparison test, comparing the mean of each group with the mean of a control group. The infected naïve mouse group was used as the control group in *D* and *E*, and the H3 group was used as the control group in *F–H* (*$P < 0.05$; **$P < 0.01$; ***$P < 0.001$; ****$P < 0.0001$; ns represents no significance, $P > 0.05$).

Influenza mucosal immunity could confer broad cross-protection against heterologous and heterosubtypic viruses. I.n. vaccination with recombinant HA vaccines is a safe and promising strategy in the generation of mucosal immunity and the prevention of influenza virus infection. However, the efficacy of i.n.-administrated protein vaccines is challenged by the harsh and tolerogenic nasal epithelium. Nanoparticle-based vaccines have the potential to overcome obstacles associated with i.n. vaccine delivery.

GO nanoparticles are a type of 2D sheet-like nanomaterials that have demonstrated superior attributes for drug delivery, including ultra-large surface area, easy modification, and excellent physiological biocompatibility. We generated a GO-based influenza vaccine nanoplatform by functionalizing GO with branched PEI for i.n. vaccination. Subsequently, we constructed influenza GP nanoparticles in a simple, easily manipulated, and productive mixing/adsorption approach. This vaccine platform possesses multiple features favorable for enhancing i.n. vaccines' immunogenicity, including high antigen-loading capacity, mucoadhesive and positive particle surface, and good flexibility for various vaccine components. With immunoenhancing features synergizing in the same particles, GP nanoparticle vaccines facilitate a comprehensive immune response, as seen in the study.

Antibody response to influenza HA is an essential attribute for vaccines designed to prevent influenza virus infection (32, 35). Enhancing the magnitude and breadth of antibody responses is critical for developing highly efficient and broadly protective influenza vaccines. We found that influenza GP nanoparticles (GP-H3 and GP-H3/CpG) vaccination potently boosted the antibody responses in systemic sites and mucosal surfaces. We observed significantly increased antigen-specific IgG levels, HAI titers, and microneutralization titers in mouse immune sera of influenza GP nanoparticle groups than the soluble H3 group. We also detected substantially enhanced cross-reactive antibody titers against the heterologous Phi and Wis viruses. Moreover, high-level IgG antibodies were induced against the conserved HA stalk antigen, indicating more broad protection. On the other hand, the "antigen reservoir" effect was discovered in GO nanoparticles in previous studies (36). The cross-reactive IgG antibodies in mouse sera may benefit from the improved antigen sustainability necessary for B cell somatic hypermutation/affinity maturation and class switching in germinal centers, particularly for weakly immunogenic HA stalk regions (37). Fc-mediated effector mechanisms, such as antibody-dependent cellular cytotoxicity and antibody-dependent cellular phagocytosis, might contribute to cross-protection (38, 39).

Mucosal immunity driven by IgA is one of the major contributors to influenza virus protection. sIgA is highly effective at preventing influenza infection at the portal of virus entry. As

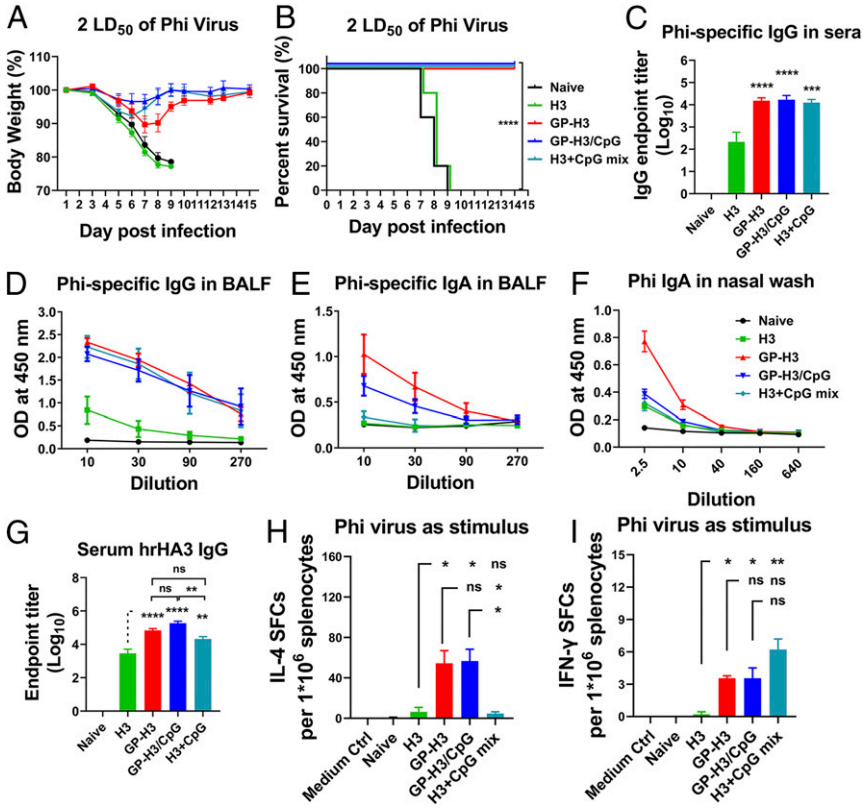

Fig. 6. Protective efficacy against heterologous influenza virus challenge. (*A*) Morbidity and (*B*) mortality of mice after challenge. (*C*) Cross-protective IgG endpoint titers against the Phi virus in mice boost sera. (*D* and *E*) Phi virus-specific IgG and IgA levels in BALF. (*F*) Phi virus-specific IgA levels in nasal washes. (*G*) Serum hrHA3-specific antibody levels. (*H* and *I*) IL-4– and IFN-γ–secreting splenocytes under inactivated Phi virus stimulation. The data are presented as mean ± SEM. The statistical significance was analyzed by one-way ANOVA followed by Tukey's multiple comparison test (*$P < 0.05$; **$P < 0.01$; ***$P < 0.001$; ****$P < 0.0001$; ns represents no significance, $P > 0.05$).

sIgA is more broadly reactive than IgG (40), the induced sIgA in GP nanoparticle groups is also a critical component of the protective scenario against various influenza virus infections. The sIgA antibodies in the mucosal washes revealed improved antibody-binding breadth as well. As an outcome, the improved antibody breadth conferred the increased cross-protection efficacy in GP nanoparticle-immunized mice.

Cellular responses play crucial roles in the fight against influenza virus infections. T helper cells are the central players in organizing an effective immune response. The differentiation of naive helper T cells into subtypes is programmed by a specific cytokine niche. TNF-α, as one of the most critical proinflammatory cytokines in cellular immunity, attracts the migration of immune cells, enhancing immune responses. IL-6 could promote the production of IL-4, a potent cytokine that directs Th2 differentiation. We found that influenza GP nanoparticles boosted the output of TNF-α and IL-6 in JAWS II DC cultures. Moreover, the nanoparticle vaccination dramatically increased the generation of IL-4–secreting cells in mouse spleens and cervical lymph nodes. IL-4 can facilitate the proliferation and differentiation of B cells into ASCs. These results were in agreement with the elevated antigen-specific IgG and IgA ASC populations observed. IFN-γ is critical in modulating cellular immunity and coordinating numerous protective functions in virus infection. We also observed significantly more IFN-γ–producing lymphocytes, which contributed to both homologous and heterologous protection in GP nanoparticle vaccination.

We observed strong cellular responses by GP nanoparticle immunization, including CD8+ T cell responses. Intracellular cytoplasmatic antigen localization is a prerequisite for the cross-presentation of extracellular antigens to CD8+ T cells by MHC I molecules (41, 42). Previous studies revealed that GO-based nanoparticles could specifically traffick through an intracellular cytosolic pathway because of the capability to destabilize intracellular vesicle lipid membranes (43, 44) or via GO-triggered autophagy (37). Moreover, it is well-documented that PEI could induce endosomal escape because of the "proton sponge effect" (45). These intriguing physicochemical characteristics of GP nanoparticles may contribute to the CD8 T cell responses and the heterologous protection observed.

As vaccine delivery carriers, GP nanoparticles could simultaneously deliver antigens and adjuvants. The large surface area and high loading capability of GP nanoparticles facilitated multiple antigens displayed on the surface, resulting in robust interaction with immune cells through multivalent recognitions. In addition to the role as a delivery carrier, GP nanoparticles exhibited immunostimulating effects. We demonstrated that GP nanoparticles significantly promoted antigen internalization in DCs, boosted proinflammatory cytokine production, and stimulated DC maturation. We observed that antigen-free GP nanoparticles enhanced DCs generation of IL-6 and expression of CD86, indicating an inherent immunostimulating effect of the particles themselves. As GO can destabilize intracellular vesicle lipid membranes (such as endolysosome) and initiate damage-associated molecular pattern innate signaling cascades (43, 44), the signaling pathway activation may partially contribute to the observed immunostimulating effects of GP nanoparticles. Otherwise, the GP nanoparticle adjuvant effect deserves to be studied in the future.

CpG ODN is an acknowledged potent mucosal immunomodulator. Despite the excellent adjuvanticity, CpG has not been approved for human use due to the safety concerns, such as activating

autoreactive B cells and increasing the risk of autoimmune disease (46) and the variable magnitude of immune effects in clinical trials (28). In the absence of any additional adjuvant, the GP nanoparticle significantly boosted antigen-specific immune responses, conferring complete protection in mice against influenza infection, comparable to the role of CpG in the H3+CpG mix. The GP nanoparticles can function as a self-adjuvanted vaccine platform. The strong self-adjuvant effect of GP nanoparticles masked the role of CpG coincorporated.

As an emerging biomaterial, the safety profiles, including the long-term accumulation and clearance of the GP nanoparticles, need further systematic preclinical evaluation. Previous studies indicated that GO nanoparticles could be degraded in the presence of human peroxidase (14). Intravenously injected GO-PVP nanosheets were excreted in the urine and cleared in the intraorgans (47). However, some other studies demonstrated that the GO nanoparticles were retained in the body for 4 wk after multiple intraperitoneal injections with a high dose (4 mg nanoparticles/kg body weight) in Wistar rats or mice (15, 48), despite no toxic effects being found on blood parameters and the health and growth of the animals. Carbon nanomaterials have also been shown to induce asbestos-like pathogenicity (49). Therefore, whether GP nanoparticles would be persistent in lungs indefinitely remains a question at present. Despite no apparent adverse effect observed in our simple safety study, a more comprehensive evaluation is needed before future clinical trials. Nevertheless, our study gives insights into developing high-performance i.n. vaccine systems with 2D sheet-like nanoparticles.

In summary, we generated influenza HA/GP nanoparticles for high-performance i.n. influenza vaccination. The functionalized GP nanoparticle served as a robust delivery/adjuvant system, significantly enhancing the recombinant HA immunogenicity. Immunization with influenza GP nanoparticles significantly boosted the magnitude and breadth of immune responses, conferring both homo- and heterologous protection. The GP nanoparticle showed enormous potential as a candidate for developing i.n. vaccines. With high versatility and flexibility, the GP nanoparticles could be easily adapted for constructing mucosal vaccines for different respiratory infectious pathogens.

Materials and Methods

Experimental Design. The objective of this study was to develop a generation of safe, efficient, and virus-independent influenza i.n. vaccines that induce cross-protection. To this end, we developed GO-based recombinant influenza HA nanoparticle vaccines. To validate the immunoenhancing effects of these vaccines, we studied their interaction with JAWS II DCs. We further evaluated the immune responses and prophylaxis protection against both homologous and heterologous influenza strains in mice after i.n. immunization with these nanoparticles. The number of mice per experimental group is indicated in the method. Statistical analyses were conducted when applicable and were included in the figure legends. All animal experiments were performed in compliance with the Institutional Animal Care and Use Committee guidelines of Georgia State University.

Materials. GO powder, branched PEI with an average molecular weight of 60 kDa, and *N*-(3-dimethyl aminopropyl-*N*-ethylcarbodiimide) hydrochloride (EDC) were purchased from Sigma-Aldrich. CpG ODN1826 was bought from InvivoGen. CFSE and BS3 were bought from Invitrogen.

Cell Lines and Viruses. Spodoptera frugiperda (Sf9, American Type Culture Collection (ATCC), CRL-1711) insect cells, JAWS II murine DCs (ATCC CRL-11904), and Madin–Darby Canine Kidney cells (MDCK (NBL-2), ATCC CCL-34) were grown in conditions recommended by the vendor.

Aic, Phi, Wis, and rSH influenza viruses were expanded in embryonated chicken eggs. Mouse-adapted Aic and Phi were prepared as lung homogenates from i.n.-infected mice. The LD_{50} was determined by the method of Reed and Muench.

Expression, Purification, and Characterization of Recombinant Trimeric HA. GCN4-stabilized Aic HA (H3) was expressed in Sf9 cells by a Bac-to-Bac baculovirus expression system (Invitrogen) and purified by a His-tag affinity method using Ni-NTA resins, as described previously (24). SDS-PAGE followed with Coomassie Blue (Bio-Rad) staining and Western blots using anti-Aic HA antibodies was performed to verify the purified H3. The H3 concentration was determined by a bicinchoninic acid assay kit (Thermo Fisher Scientific). HA trimerization was determined by BS3 cross-linking at different concentrations (0, 0.5, 5, and 10 mM) followed by Western blots as previously described (50).

Preparation of GO and GP Nanoparticles. GO nanoparticles were prepared from GO powder by tip ultrasonication. Briefly, GO powder was resuspended in Milli-Q water and then sonicated at 100 W in an ice bath for 2 h. GO particle size was measured at different sonication time intervals by dynamic light scattering (DLS) with a Malvern Zetasizer Nano ZS (Malvern Instruments). The final GO solution was centrifuged at 6,000 rpm for 5 min to remove larger particles.

We prepared GP nanoparticles by using Carbodiimide coupling method. Ten milliliters of GO solution (0.5 mg/mL) was sonicated for 30 min, and then 0.6 mL of PEI solution (50 mg/mL) was added and sonicated for another 30 min. The mixture was activated by adding two batches of EDC (50 mg) at an interval of 30 min followed by stirring at room temperature overnight. GP nanoparticles were collected by centrifugation at 15,000 rpm at 4 °C for 2 h and then repeatedly washed with Milli-Q water to remove the free PEI. GP nanoparticle pellets were resuspended in pure water and stored at 4 °C in dark for later use. The concentrations of GO and GP nanoparticles were determined by their absorbances at 230 nm with a Nanodrop spectrometer (Thermo Fisher Scientific), according to the Beer–Lambert law ($A = \varepsilon lc$). Herein, the mass extinction coefficient (ε) of GO was set as 65 mL $\cdot$ mg^{-1} $\cdot$ cm^{-1}, as previously reported (18).

Fabrication and Optimization of GP-H3 and GP-H3/CpG Nanoparticles. GP-based vaccine formulations were prepared by a simple mixing/adsorption approach. The loading capability of H3 on the GP nanoparticles was evaluated via reducing SDS-PAGE. We prepared a series of GP-H3 nanoparticles at six different weight ratios (2:1, 1:1, 1:2, 1:4, 1:6, and 1:8) under stirring for 20 min at room temperature. The GP-H3 nanoparticles were collected by centrifugation at 15,000 rpm for 20 min and then dispersed in an equal amount of phosphate-buffered saline (PBS). The supernatants were kept separately. Both the nanoparticles and supernatants for all the formulations were analyzed by 10% SDS-PAGE. The gel was stained with Coomassie blue and imaged with the ChemiDoc Touch imaging system (Bio-Rad).

In some formulations, CpG was coloaded onto GP nanoparticles with antigens. We employed agarose gel electrophoresis to investigate whether all the feeding CpG were complexed and loaded onto the GP nanoparticles. Soluble CpG, GP-H3/CpG (10:5:1), GP-H3/CpG (10:5:2.5), and H3+CpG mix were centrifuged at 15,000 rpm for 20 min, and the supernatants were analyzed by 1% agarose gel electrophoresis. The gel was visualized with ChemiDoc Touch imaging system (Bio-Rad) to determine the existence of CpG in the supernatants.

Nanoparticle Characterization. Particle sizes and Zeta potentials of the resulting nanoparticles were measured by DLS. The GO nanoparticle morphology was characterized by AFM with a Bruker Icon AFM and TEM with a JEOL 100 CX-II. UV-Vis absorption spectra of the samples were recorded by a Nanodrop spectrometer (Thermo Fisher Scientific). TGA of the GO and GP nanoparticles was performed using a TA Q500 instrument under an inert nitrogen atmosphere. The heating rate and nitrogen flow rate were 10 °C/min and 50 mL/min, respectively. The maximum temperature was 600 °C.

Cellular Uptake in JAWS II Cells by Immunofluorescence Imaging. The internalization profiles of soluble H3 and GP-H3 nanoparticles in JAWS II cells were studied by immunofluorescence imaging. JAWS II cells were seeded at 2×10^5 cells/well (2×10^5 cells/mL, 1 mL) in a 24-well cell culture plate and treated with soluble H3 or GP-H3 nanoparticles at an H3 concentration of 10 μg/mL. Untreated cells were used as negative controls. After 16-h incubation, the cells were washed twice with Dulbecco's PBS and then fixed and permeabilized with BD fixation/permeabilization buffer at 4 °C for 20 min, followed by blocking with 5% bovine serum albumin for 1 h at room temperature. After washing twice more, the cells were stained successively with antigen-specific antibodies for 1 h and fluorescent DyLight 649-conjugated goat anti-mouse IgG antibodies (BioLegend) for 30 min. The cells were recorded by using a Keyence BZ-X710 fluorescence microscope.

Proinflammatory Cytokine Profiles and Maturation of Stimulated JAWS II Cells. JAWS II cells were seeded at 4×10^4 cells/well (4×10^5 cells/mL, 100 μL/well) in a 96-well cell culture plate, followed by treatment with soluble H3, GP, GP-H3,

GP-H3/CpG, or H3+CpG mix formulations for 16 h. The final concentration of H3 was 5 or 10 μg/mL. The ratio of GP:H3:CpG was 10:5:1 (w:w:w). Untreated cells were used as negative controls. Supernatants were collected for determining IL-6 and TNF-α levels by using cytokine ELISA kits (Thermo Scientific). Cells were collected for evaluating the maturation of stimulated JAWS II cells. The cell surface marker CD86 was determined by flow cytometry, as previously described (51). Data were analyzed with the FlowJo software.

Immunization, Sample Collection, and Challenge. Female BALB/c mice (6 ~ 8 wk old, $n = 20$) were i.n.-immunized with 30 μL of soluble H3, GP-H3, GP-H3/CpG, or H3+CpG in saline (5 μg of H3 protein per mouse). Mice were vaccinated twice at an interval of 4 wk.

Prime sera were collected 3 wk post-priming immunization, and boost sera were collected 3 wk post-boosting immunization ($n = 7$). Nasal washes and BALF ($n = 3$ to 4) were collected 3 wk after boosting immunization by flushing the respective cavities with 1 mL of cold sterile PBS and then centrifuged at 10,000 rpm for 5 min. Spleens, CLNs, and NALTs of the immunized mice ($n = 4$) were isolated 3 wk after boosting immunization. Single-cell suspensions were obtained by gently grinding tissues with frosted microscope slides. Splenocytes were harvested after treating with red blood cell lysis buffer.

Mice ($n = 5$) were i.n.-challenged with 15× LD_{50} of mouse-adapted Aic or 2× LD_{50} of Phi in 30 μL saline 4 wk after the boosting immunization. Mouse body weight loss and survival rates were recorded daily for 2 wk postinfection. A weight loss exceeding 20% was used as a humane endpoint. Mice were killed and lung tissues were isolated for lung viral titer determination and histological analysis 5 d postinfection with Aic.

Safety Evaluation of GP-H3 Nanoparticles. Mouse body weight was monitored for 7 d postvaccination. Histological examination of mouse nasal mucosa and lung tissues was performed with hematoxylin and eosin (H&E) staining 24 h and 7 d postvaccination, respectively. The nasal cavities were decalcified with ethylene diamine tetraacetic acid disodium salt solution, followed by cryosectioning and H&E staining. Lung tissues were paraffin embedded, followed by sectioning and H&E staining.

Antibody ELISA, HAI Assay, and Viral Neutralization Assay. Antibody ELISA was performed as previously described (52). The virus (Aic, Phi, Wis, or rSH) or H3-specific IgG, IgA, or IgE antibody endpoint titers in sera, nasal washes, or BALF samples postimmunization were tested. The highest dilution with an OD_{450} twice that of the naive group was used as the endpoint titer. HAI titers of mouse boost immune sera were determined as previously described (53). Sera samples were pretreated with receptor destroying enzyme (Denka Seiken Co., Ltd) overnight at 37 °C and then heat inactivated at 56 °C for 30 min before the test. Turkey red blood cells (0.5%) were used for this assay, and the highest dilution able to inhibit virus hemagglutination was used as the HAI titer.

The median $TCID_{50}$ of Aic and Phi viruses were determined according to Reed and Muench method. Twofold serial dilutions of heat-inactivated (56 °C for 30 min) mouse boost immune sera in Eagle's minimal essential medium (EMEM) (50 μL) were mixed with 100-fold $TCID_{50}$ of Aic or Phi virus in EMEM (50 μL) for 2 h at 37 °C. After incubation, the mixture was added to MDCK cell monolayers (100 μL/well, 1.5×10^5 cells/mL, with 2 μg/mL of TBCK-trypsin) and incubated for 3 d at 37 °C. A standard hemagglutination assay was used to determine virus inhibition.

Enzyme-Linked Immunospot Assay. Cytokine Enzyme-linked immunospot (ELISpot) assay (BioLegend) was performed to analyze IL-4– or IFN-γ–secreting cells. Briefly, splenocytes or CLN cells (3×10^6 cells/mL, 100 μL/well) were seeded into 96-well filtration plates (MultiScreen-HA, Millipore) that were pretreated with anti-mouse IFN-γ or IL-4 antibodies and then stimulated with H3 (4 μg/mL) for 24 h at 37 °C. After removing cells, plates were incubated with biotin-conjugated IFN-γ or IL-4 detection antibody at 37 °C for 1 h, followed by the addition of horseradish peroxidase (HRP)-streptavidin for another 1 h. True Blue Peroxidase substrate (KPL) was used to develop spots, and spots were recorded with Bioreader-6000-E (BIOSYS).

B cell ELISpot assay was used to evaluate the antigen-specific ASCs. Briefly, 96-well filtration plates were precoated with H3 proteins (50 μL/well, 4 μg/mL) overnight at 4 °C, washed, blocked, and then splenocytes or NALT cells (3×10^6 cells/mL, 100 μL/well) were seeded and incubated overnight at 37 °C. After removing cells, HRP-conjugated anti-mouse IgG or IgA antibodies were added for 1 h at room temperature. True Blue Peroxidase substrate was used to develop spots. Results were recorded with Bioreader-6000-E.

Proliferation Assay by CFSE Staining. The proliferation ability of splenocytes was evaluated by using the CFSE Cell Proliferation Assay Kit (Invitrogen). Splenocytes were stained with CFSE at 37 °C for 10 min, washed with complete Roswell Park Memorial Institute medium 1640 thoroughly, and then seeded into 24-well plates (1×10^6 cells/well) and incubated with H3 (5 μg/mL) for 60 h. The cells were then harvested and stained for 30 min at 4 °C with anti-mouse PE-Cy7-anti-CD4 and PE-Cy5-anti-CD8α antibodies (Biolegend) in the presence of Fc blocker. After washing and resuspending in flow cytometry staining buffer (PBS + 5% fetal calf serum), the cells were measured with a BD LSRFortessa flow cytometer (BD biosciences). Data were analyzed using the FlowJo software (FlowJo LLC). The splenocytes from naïve mice were used as control.

Analysis of T Cell Subpopulations. The CD3+CD4+ and CD3+CD8+ T cell subpopulations in spleens of immunized mice were analyzed by flow cytometry. Briefly, splenocyte suspensions (1×10^6 cells/mL, 1 mL/well) were seeded into 24-well plates and restimulated with H3 (5 μg/mL) for 36 h at 37 °C. The cells were harvested and stained for 30 min at 4 °C with PE-anti-CD3ε, PE-Cy7-anti-CD4, and PE-Cy5-anti-CD8α antibodies. After washing and resuspending in flow cytometry staining buffer, the cells were detected with a BD LSRFortessa flow cytometer and analyzed with the FlowJo software.

Histological Analysis After Virus Infection. On day 5 postinfection with Aic virus, mice were euthanized. Lung tissues were isolated, fixed with 10% neutral buffered formalin overnight at 4 °C, dehydrated, and then embedded in paraffin, followed by sectioning and H&E staining. The tissue sections were recorded by a Keyence BZ-X710 microscope and examined by five unbiased pathologists. The degree of leukocyte infiltration was scored on a scale of 0 to 5. Scores were given as absent (0), subtle (1), mild (2), moderate (3), severe (4), and massive (5).

Lung Viral Titration. Lung tissues were homogenized and supernatants were cleared by centrifugation at 10,000 rpm for 10 min at 4 °C 5 d postinfection with the Aic virus. The 10-fold serial dilutions of lung supernatants (100 μL) were added to the prepared 96-well plates containing MDCK cells (1.5×10^5 cells/mL, 100 μL) and cocultured for 5 d. A standard hemagglutination assay was carried out to determine viral titers in the supernatants by the Reed–Munchen method.

Evaluation of Inflammatory Cytokine Levels in BALF. To evaluate the pulmonary immunopathology caused by a virus infection, inflammatory cytokine (TNF-α, IL-12, and IL-6) levels in the BALF of infected mice were measured according to the cytokine ELISA kit's instructions (Thermo Scientific).

Statistical Analysis. All data were represented as means with the SEM. Statistical significance was analyzed by the one-way ANOVA. A probability value (P) of less than 0.05 is considered statistically significant. Survival rate statistical analysis was performed with the Log-rank (Mantel–Cox) test. The analysis was performed with GraphPad Prism 8 program (GraphPad software).

Data Availability. All study data are included in the article and/or *SI Appendix*.

ACKNOWLEDGMENTS. This work was supported by the US NIH/National Institute of Allergy and Infectious Diseases under Grants R01AI101047, R01AI116835, and R01AI143844 to B.-Z.W. The electron microscopy study was performed in part at the Georgia Institute of Technology for Electronics and Nanotechnology, a member of the National Nanotechnology Coordinated Infrastructure supported by the NSF (Grant ECCS-1542174). The content in this study is solely our responsibility and does not necessarily represent the official views of the funders.

1. C. Calzas, C. Chevalier, Innovative mucosal vaccine formulations against influenza A virus infections. *Front. Immunol.* **10**, 1605 (2019).
2. M. A. Rose, S. Zielen, U. Baumann, Mucosal immunity and nasal influenza vaccination. *Expert Rev. Vaccines* **11**, 595–607 (2012).
3. D. S. Rajão, D. R. Pérez, Universal vaccines and vaccine platforms to protect against influenza viruses in humans and agriculture. *Front. Microbiol.* **9**, 123 (2018).
4. E. C. Lavelle, Generation of improved mucosal vaccines by induction of innate immunity. *Cell. Mol. Life Sci.* **62**, 2750–2770 (2005).
5. K. A. Woodrow, K. M. Bennett, D. D. Lo, Mucosal vaccine design and delivery. *Annu. Rev. Biomed. Eng.* **14**, 17–46 (2012).
6. K. T. Gause *et al*., Immunological principles guiding the rational design of particles for vaccine delivery. *ACS Nano* **11**, 54–68 (2017).

7. Z. R. Sia, M. S. Miller, J. F. Lovell, Engineered nanoparticle applications for recombinant influenza vaccines. *Mol. Pharm.* **18**, 576–592 (2021).
8. J. Wang *et al*., Pulmonary surfactant-biomimetic nanoparticles potentiate heterosubtypic influenza immunity. *Science* **367**, eaau0810 (2020).
9. T. Nochi *et al*., Nanogel antigenic protein-delivery system for adjuvant-free intranasal vaccines. *Nat. Mater.* **9**, 572–578 (2010).
10. S. Li *et al*., Polyethylenimine-modified fluorescent carbon dots as vaccine delivery system for intranasal immunization. *ACS Biomater. Sci. Eng.* **4**, 142–150 (2018).
11. A. Sinha *et al*., Carbohydrate-functionalized rGO as an effective cancer vaccine for stimulating antigen-specific cytotoxic T cells and inhibiting tumor growth. *Chem. Mater.* **29**, 6883–6892 (2017).
12. L. A. Dykman, Gold nanoparticles for preparation of antibodies and vaccines against infectious diseases. *Expert Rev. Vaccines* **19**, 465–477 (2020).
13. M. Kanekiyo *et al*., Self-assembling influenza nanoparticle vaccines elicit broadly neutralizing H1N1 antibodies. *Nature* **499**, 102–106 (2013).
14. R. Kurapati *et al*., Dispersibility-dependent biodegradation of graphene oxide by myeloperoxidase. *Small* **11**, 3985–3994 (2015).
15. K. Yang *et al*., In vivo biodistribution and toxicology of functionalized nano-graphene oxide in mice after oral and intraperitoneal administration. *Biomaterials* **34**, 2787–2795 (2013).
16. Y. Cao *et al*., Ultrasmall graphene oxide supported gold nanoparticles as adjuvants improve humoral and cellular immunity in mice. *Adv. Funct. Mater.* **24**, 6963–6971 (2014).
17. C. Meng *et al*., Graphene oxides decorated with carnosine as an adjuvant to modulate innate immune and improve adaptive immunity in vivo. *ACS Nano* **10**, 2203–2213 (2016).
18. L. Xu *et al*., Functionalized graphene oxide serves as a novel vaccine nano-adjuvant for robust stimulation of cellular immunity. *Nanoscale* **8**, 3785–3795 (2016).
19. V. Georgakilas *et al*., Noncovalent functionalization of graphene and graphene oxide for energy materials, biosensing, catalytic, and biomedical applications. *Chem. Rev.* **116**, 5464–5519 (2016).
20. M. C. Demirel, M. Vural, M. Terrones, Composites of proteins and 2D nanomaterials. *Adv. Funct. Mater.* **28**, 1704990 (2018).
21. C. A. Fromen *et al*., Controlled analysis of nanoparticle charge on mucosal and systemic antibody responses following pulmonary immunization. *Proc. Natl. Acad. Sci. U.S.A.* **112**, 488–493 (2015).
22. F. Wegmann *et al*., Polyethyleneimine is a potent mucosal adjuvant for viral glycoprotein antigens. *Nat. Biotechnol.* **30**, 883–888 (2012).
23. L. Feng, S. Zhang, Z. Liu, Graphene based gene transfection. *Nanoscale* **3**, 1252–1257 (2011).
24. W. C. Weldon *et al*., Enhanced immunogenicity of stabilized trimeric soluble influenza hemagglutinin. *PLoS One* **5**, e12466 (2010).
25. Y.-L. Lin *et al*., A CpG-adjuvanted intranasal enterovirus 71 vaccine elicits mucosal and systemic immune responses and protects human SCARB2-transgenic mice against lethal challenge. *Sci. Rep.* **8**, 10713 (2018).
26. R. J. Hopkins *et al*., Randomized, double-blind, placebo-controlled, safety and immunogenicity study of 4 formulations of Anthrax Vaccine Adsorbed plus CPG 7909 (AV7909) in healthy adult volunteers. *Vaccine* **31**, 3051–3058 (2013).
27. D. Rynkiewicz *et al*., Marked enhancement of the immune response to BioThrax® (Anthrax Vaccine Adsorbed) by the TLR9 agonist CPG 7909 in healthy volunteers. *Vaccine* **29**, 6313–6320 (2011).
28. J. Scheiermann, D. M. Klinman, Clinical evaluation of CpG oligonucleotides as adjuvants for vaccines targeting infectious diseases and cancer. *Vaccine* **32**, 6377–6389 (2014).
29. S. E. Ohmit, J. G. Petrie, R. T. Cross, E. Johnson, A. S. Monto, Influenza hemagglutination-inhibition antibody titer as a correlate of vaccine-induced protection. *J. Infect. Dis.* **204**, 1879–1885 (2011).
30. H. O. Padilla-Quirarte, D. V. Lopez-Guerrero, L. Gutierrez-Xicotencatl, F. Esquivel-Guadarrama, Protective antibodies against influenza proteins. *Front. Immunol.* **10**, 1677 (2019).
31. Y. Asahi-Ozaki *et al*., Secretory IgA antibodies provide cross-protection against infection with different strains of influenza B virus. *J. Med. Virol.* **74**, 328–335 (2004).
32. F. Krammer, The human antibody response to influenza A virus infection and vaccination. *Nat. Rev. Immunol.* **19**, 383–397 (2019).
33. L. Wang *et al*., Nanoclusters self-assembled from conformation-stabilized influenza M2e as broadly cross-protective influenza vaccines. *Nanomedicine (Lond.)* **10**, 473–482 (2014).
34. T. Saito *et al*., Effective collaboration between IL-4 and IL-21 on B cell activation. *Immunobiology* **213**, 545–555 (2008).
35. W. Smith, C. H. Andrewes, P. P. Laidlaw, A virus obtained from influenza patients. *Lancet* **222**, 66–68 (1933).
36. H. Yue *et al*., Exploration of graphene oxide as an intelligent platform for cancer vaccines. *Nanoscale* **7**, 19949–19957 (2015).
37. H. H. Tam *et al*., Sustained antigen availability during germinal center initiation enhances antibody responses to vaccination. *Proc. Natl. Acad. Sci. U.S.A.* **113**, E6639–E6648 (2016).
38. D. J. DiLillo, P. Palese, P. C. Wilson, J. V. Ravetch, Broadly neutralizing anti-influenza antibodies require Fc receptor engagement for in vivo protection. *J. Clin. Invest.* **126**, 605–610 (2016).
39. N. L. Kallewaard *et al*., Structure and function analysis of an antibody recognizing all influenza A subtypes. *Cell* **166**, 596–608 (2016).
40. T. Suzuki *et al*., Relationship of the quaternary structure of human secretory IgA to neutralization of influenza virus. *Proc. Natl. Acad. Sci. U.S.A.* **112**, 7809–7814 (2015).
41. S. Burgdorf, C. Schölz, A. Kautz, R. Tampé, C. Kurts, Spatial and mechanistic separation of cross-presentation and endogenous antigen presentation. *Nat. Immunol.* **9**, 558–566 (2008).
42. J. M. Vyas, A. G. Van der Veen, H. L. Ploegh, The known unknowns of antigen processing and presentation. *Nat. Rev. Immunol.* **8**, 607–618 (2008).
43. Y. Tu *et al*., Destructive extraction of phospholipids from Escherichia coli membranes by graphene nanosheets. *Nat. Nanotechnol.* **8**, 594–601 (2013).
44. H. Li *et al*., Spontaneous protein adsorption on graphene oxide nanosheets allowing efficient intracellular vaccine protein delivery. *ACS Appl. Mater. Interfaces* **8**, 1147–1155 (2016).
45. S. S. Rohiwal *et al*., Polyethylenimine based magnetic nanoparticles mediated non-viral CRISPR/Cas9 system for genome editing. *Sci. Rep.* **10**, 4619 (2020).
46. A. M. Krieg, J. Vollmer, Toll-like receptors 7, 8, and 9: Linking innate immunity to autoimmunity. *Immunol. Rev.* **220**, 251–269 (2007).
47. S. Liang *et al*., In vivo pharmacokinetics, transfer and clearance study of graphene oxide by La/Ce dual elemental labelling method. *NanoImpact* **17**, 100213 (2020).
48. N. Kurantowicz *et al*., Biodistribution of a high dose of diamond, graphite, and graphene oxide nanoparticles after multiple intraperitoneal injections in rats. *Nanoscale Res. Lett.* **10**, 398 (2015).
49. C. A. Poland *et al*., Carbon nanotubes introduced into the abdominal cavity of mice show asbestos-like pathogenicity in a pilot study. *Nat. Nanotechnol.* **3**, 423–428 (2008).
50. L. Deng *et al*., Double-layered protein nanoparticles induce broad protection against divergent influenza A viruses. *Nat. Commun.* **9**, 359 (2018).
51. L. Wang *et al*., Coated protein nanoclusters from influenza H7N9 HA are highly immunogenic and induce robust protective immunity. *Nanomedicine (Lond.)* **13**, 253–262 (2017).
52. C. Wang, W. Zhu, Y. Luo, B.-Z. Wang, Gold nanoparticles conjugating recombinant influenza hemagglutinin trimers and flagellin enhanced mucosal cellular immunity. *Nanomedicine (Lond.)* **14**, 1349–1360 (2018).
53. A. Impagliazzo *et al*., A stable trimeric influenza hemagglutinin stem as a broadly protective immunogen. *Science* **349**, 1301–1306 (2015).